Understanding Non-Stick on Lead Wirebond Failure Due to Leadfinger Surface Roughness

Alexander Angeles[1], Ian Harvey Arellano[2]
[1]Assembly Manufacturing, [2]Central Engineering & Development
STMicroelectronics, Inc., 9 Mountain Drive, LISP II, Calamba 4027 Laguna, Philippines

Abstract— Non-stick on lead (NSOL) failure in the wedge bonding process of wirebonded semiconductor and electronic devices is a key issue for wedge bondability. The defect has been correlated with different factors but little has been established on the quantitative correlation with surface roughness (SR). Herein, the direct empirical correlation between SR of substrate leadfinger and the occurrence of NSOL in two (2) ball grid array (BGA) packages namely, P1 and P2 is reported and discussed. SR response was quantified by R_a (arithmetical mean SR) and R_z (10-point mean roughness) integrated over the whole surface (JIS B0601:1994 standard) using an atomic force microscope (AFM). Direct correlation has been established where high occurrence of NSOL was observed on substrates with high SR. This general correlation was found to be true for the two (2) packages evaluated in this study. R_a values of 0.192 ± 0.028 μm and R_z of 1.49 ± 0.18 μm were found to produce lower NSOL rate compared with R_a value of 0.239 ± 0.023 μm and R_z of 2.75 ± 0.52 μm for P1. Likewise, R_a of 0.272 ± 0.037 μm and R_z of 3.00 ± 0.57 μm were found to have higher occurrence of NSOL compared with R_a of 0.239 ± 0.037 μm and R_z of 2.34 ± 0.32 μm for P2.

Keywords— Surface roughness, non-stick on leads, wirebond, wedge bond.

I. Introduction

Wirebonding (WB) continues to occupy about 90% of first level chip interconnection due to its cost effectiveness and technological maturity [1-6]. The connection integrity relies on the wirebonding process robustness that depends, in turn, on the attachment of the wire on the pad and the carrier lead fingers. Factors such as bond pad size, bond pad pitch, wire diameter, bonding surfaces, metallization, loop height, loop length, bonder speed and accuracy, and package design affect the occurrence of defects, and the performance of the wirebond process. Common defects encountered at this process station are lifted stitch/non-stick on leads (NSOL), non-stick on pads (NSOP), and the presence of contamination or foreign material, plating defects, cut wire and missing wires, among others. NSOL has been classified as the top defect contributor for the two BGA packages reported herein. NSOL occurs when the interface between the carrier leadfinger and the stitch is not robust enough to stand the forces acting upon the interface. The nature of the surface finish is a potent contributor to the interfacial robustness. Hence, surface roughness (SR) could be correlated with the occurrence of this surface-related defect.

The measurement of the SR has been used for many years as a means of expressing or examining the quality of the surface in the manufacturing industry [7-10]. The definition of surface roughness is expressed by the microcosmic geometrical shape characteristic of some wave crests and wave troughs on the manufactured surface, among which there is smaller space [11]. The technology advancement towards the smaller dimensional scale of nanometers and sub-micon levels necessitates new instrumentations that could perform with resolutions at this scale. In 1982, Gerd Binnig and Heinrich Rohrer and their colleagues at the Zurich Research Laboratory of the International Business Machines (IBM) developed a new kind of surface analytical instrument, the Scanning Tunneling Microscope (STM). The emergence of STM makes it possible to observe the arrangement of individual atoms on the material surface, and the physical and chemical properties related to the behavior of the surface electrons in real space. Gerd Binnig and Heinrich Rohrer were awarded the Nobel Prize in Physics in1986 for their outstanding contribution to science [12-13]. Immediately following the discovery of the STM, a new class of microscopy techniques, known collectively as Scanning Probe Microscopy (SPM), was born. The method exploits the interaction between a physical probe and a surface. The interaction can be physical, chemical, electrical, magnetic, thermal or optical. Atomic Force Microscopy (AFM) is one of the techniques in this class. AFM uses the attractive or repulsive forces on the surface of a material. This method can be used to image the topography and quantitatively measure the roughness of a surface with a nanometer resolution.

In this paper, the SR measurement of the leadfingers of two types of substrates using AFM is presented. The SR was quantified using R_a and R_z values, and were statistically compared using Analysis of Variance (ANOVA) and Tukey-Kramer statistics. The measured values were correlated with the occurrence of NSOL in an attempt to increase the wirebond yield for the two BGA packages by reducing this top defect contributor.

II. Experimental Details

Materials and Methods. Two (2) BGA packages, P1 and P2 were assembled through the normal process utilizing qualified commercial materials and optimized processes. The substrate for P1 comes from three (3) different suppliers; SA, SB and SC while that of P2 comes from one supplier with 2 processing plants; H2 and H4. The yield at the wirebond (WB) process was monitored and the defect contributors were identified.

SR measurements were performed on the leadfingers of the substrates used for P1 and P2. Twenty-five (25) data points were generated randomly over the entirety of the substrate

strip. Each data point corresponds to a 50 μm by 50 μm surface. Results from a separate study established statistically non-significant point-to-point and lead-to-lead variation within a unit. Thus, a single point reading per unit is enough to produce a statistical representation of a single unit. All SR measurements were performed using Atomic Force Microscope (AFM, Park Systems XE-100) in contact mode. The probe tip used (Fig. 1) is a high mechanical Q-factor silicon with radius of curvature of less than 10 nm, a force constant of 0.20 N m^{-1} and 23 kHz resonant frequency mounted on a stainless steel cantilever. The scan was performed at a rate of 1 Hz with a setpoint of 2.90 nN.
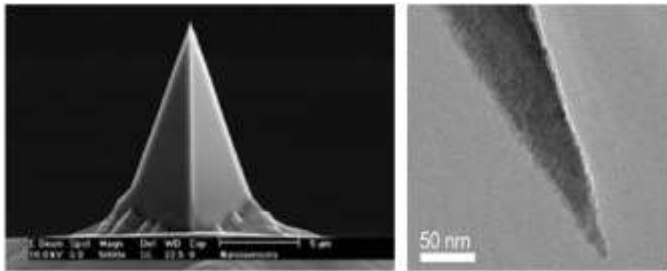

Fig. 1. Contact mode probe tip. (Image courtesy of Park Systems, Inc.).

Mathematical models of surface roughness. The roughness of each 50 μm x 50 μm surface was quantified using R_a (arithmetical average SR) and R_z (10-point mean roughness). R_a is given by the sum of the absolute values of all profile setovers in the sampling length divided by the sampling points. The R_a value is given by the following formula:

$$R_a = \frac{1}{N}\left(\sum_{i=1}^{N}|y_i|\right) \quad (1)$$

where y_i is the profile setover of the ith sampling point, N is the numbers of sampling point.

The ten-point mean roughness (R_z) is expressed by the sum of the average peak of five highest peaks and the average valley of five lowest valleys in the sampling length. The R_z value is expressed by the following formula:

$$R_z = y_p + y_v \quad (2)$$

$$y_p = \frac{|y_{p1} + y_{p2} + y_{p3} + y_{p4} + y_{p5}|}{5} \quad (3)$$

$$y_v = \frac{|y_{v1} + y_{v2} + y_{v3} + y_{v4} + y_{v5}|}{5} \quad (4)$$

where y_{p1-5} and y_{v1-5} are the 5 highest peaks and 5 lowest troughs, respectively.

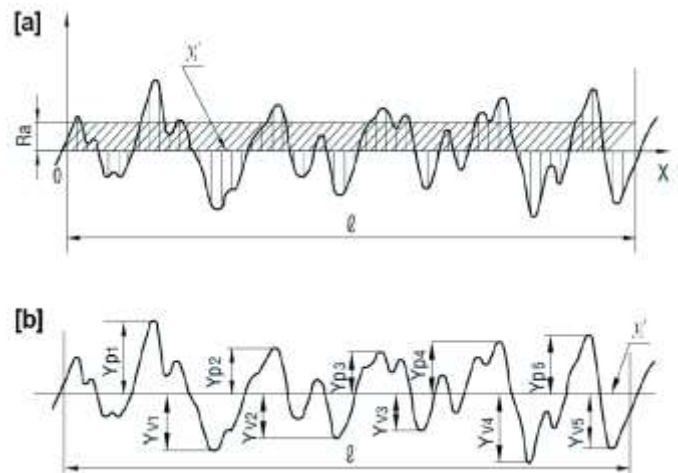These roughness parameters are geometrically represented in Fig. 2.

Fig. 2. Geometric representations of R_a and R_z [14].

In order to calculate the values of all kinds of surface roughness parameters, the datum line is supposed to be determined after obtaining the curve profile of an actual surface. In this paper, the least square centerline, y_i', belonging to the centerline system is adopted. The definition of the least square centerline is expressed by the line dividing the geometrical profile shape. The least square centerline is also the datum line, which makes the square sum of all profile setovers minimal in the sampling length. The correct determination of the least square centerline plays a decisive role in the calculation of surface roughness parameters [11].

Suppose y_{oi} is the coordinate of the ith sampling point in the vertical direction, and x_i is the coordinate of the ith sampling point in the horizontal direction; where $i = 1, 2, ..., N$. The regression equation of the least square centerline is described by the following expression:

$$y_i^{'} = ax_i + b \quad (5)$$

where a is the slope of the least square centerline and b is the intercept of the least square centerline in the vertical direction. So the profile setovers are computed by the following expression:

$$y_i = y_{oi} - y_i^{'} \quad (6)$$

According to the definition of the least square centerline, the following expression could be given:

$$\sum_{i=1}^{N} y_i^{2} = \min \quad (7)$$

So the least square equation set is represented by the following expression:

$$\begin{cases} bN + a\sum_{i=1}^{N} x_i = \sum_{i=1}^{N} y_{oi} \\ b\sum_{i=1}^{N} x_i + a\sum_{i=1}^{N} x_i^{2} = \sum_{i=1}^{N}(x_i \cdot y_{oi}) \end{cases} \quad (8)$$

By solving the least square equation set, a and b are determined by the following expression:

$$\begin{cases} a = \dfrac{\sum\limits_{i=1}^{N}(x_i \cdot y_{oi}) - \dfrac{1}{N}\left(\sum\limits_{i=1}^{N}x_i\right)\left(\sum\limits_{i=1}^{N}y_{oi}\right)}{\sum\limits_{i=1}^{N}y_i^2 - \dfrac{1}{N}\left(\sum\limits_{i=1}^{N}x_i\right)} \\[3em] b = \dfrac{1}{N}\left(\sum\limits_{i=1}^{N}y_{oi} - a\sum\limits_{i=1}^{N}x_i\right) \end{cases} \qquad (9)$$

The least square centerline is determined by replacing the values a and b in (6).

III. RESULTS AND DISCUSSION

The assembly yield of two (2) BGA packages was affected by the yield at the wirebond station. Fig. 3 shows that P1 and P2 fall short of the target yield of 99.6%. Notation in Fig. 3 is based on the substrate supplier for P1; SA, SB and SC, while P2 is based on the processing plants of the same supplier; H2 and H4. The number of lots was also indicated to show clearly the statistical validity of the data presented and to highlight the need to eliminate the factors causing the low WB yield. While at first glance the discrepancy can be considered small, in a mass manufacturing setup, this is equivalent to a large loss in business revenue. On a positive note, the condition presents an opportunity for improvement. As such, a team was formed to address the issue via DMAIC, and the results presented herein are a subset of the overall approach.
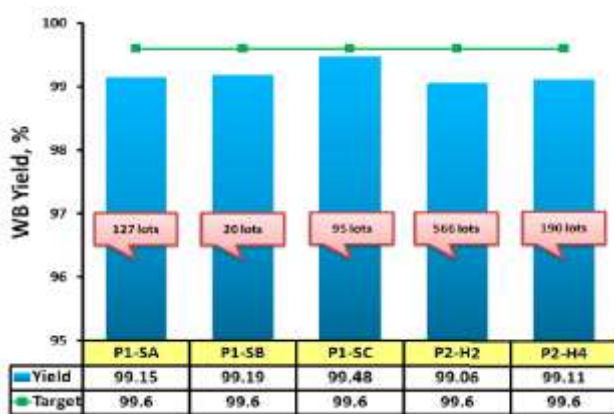

Fig. 3. Wirebond yield of P1 and P2.

In an attempt to structurally analyze the source of the problem, top defect contributors were identified, and their occurrence quantified. Fig. 4 shows the top defect distribution among the packages, and their corresponding subsets, considered in this study. It is clearly shown that lifted stitch or non-stick on leads is the top defect contributor. Hence, attention was focused in solving this problem. With a time-tested optimized process, the focus was shifted to the nature of the materials. The problem is a classic case of interface compatibility between materials where several factors could take play. The morphology of the NiAu surface finish of the leadfingers was identified as a probable source of the non-robust adhesion between the stitch and the fingers. To validate

this hypothesis, correlation between SR of the leadfingers and the NSOL occurrence was performed.

The surface roughness was measured using an AFM under contact mode. Surface topography of the 50 μm x 50 μm region for each case was imaged. Scale-normalized representative 2D and 3D images are shown in Fig. 5. These topographical images are good visual indicators of the leadfinger surface finish roughness. However, to fully utilize the functionality of this test, quantitative surface roughness analysis was performed by utilizing the mathematical models presented earlier. R_a and R_z were chosen because these two are the most used roughness parameters and were prescribed in Japanese Industrial Standards (JIS) documents. Each 50 μm by 50 μm surface have a corresponding R_a and R_z values. Statistical analysis of these values is necessary to show that the difference, if there is any, is statistically valid.
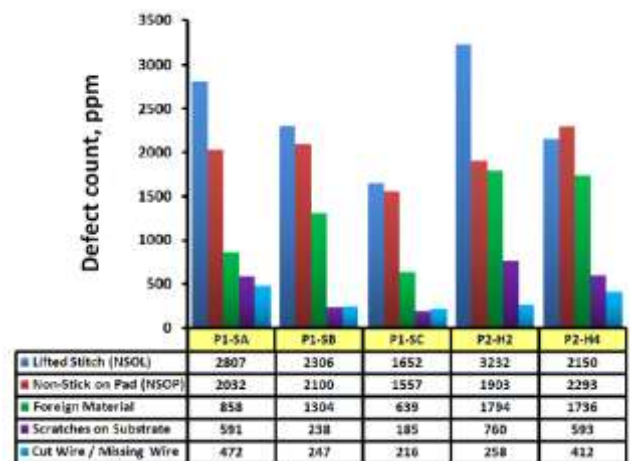

Fig. 4. Top defect contributor distribution.

Multivariate correlation test was performed for both R_a and R_z values for the five (5) data set. As shown in Fig. 6a and b, weak correlation was observed for both roughness parameter as implicated by the roundedness of the density ellipse and the low r values. These results indicate that a probable difference in the roughness parameters among the test subjects can be further tested.

Performing ANOVA in conjunction with Tukey-Kramer test show that a statistical difference exists in some cases. In P1, P1-SA exhibited significantly higher SR compared with P1-SB and P1-SC, where the latter two show similar characteristics. This observation is shown in Fig. 7a and b, and is true for both SR parameters, R_a and R_z.

Performing the same analysis for P2, Fig. 8a and b, show that P2-H2 has a statistically higher SR compared with P2-H4 for both roughness parameters. Please note that the comparative analysis was performed per package type because the package-to-package comparison is not feasible due to the weak correlation established from Fig. 6, and the difference in the bonding parameters used for P1 and P2.
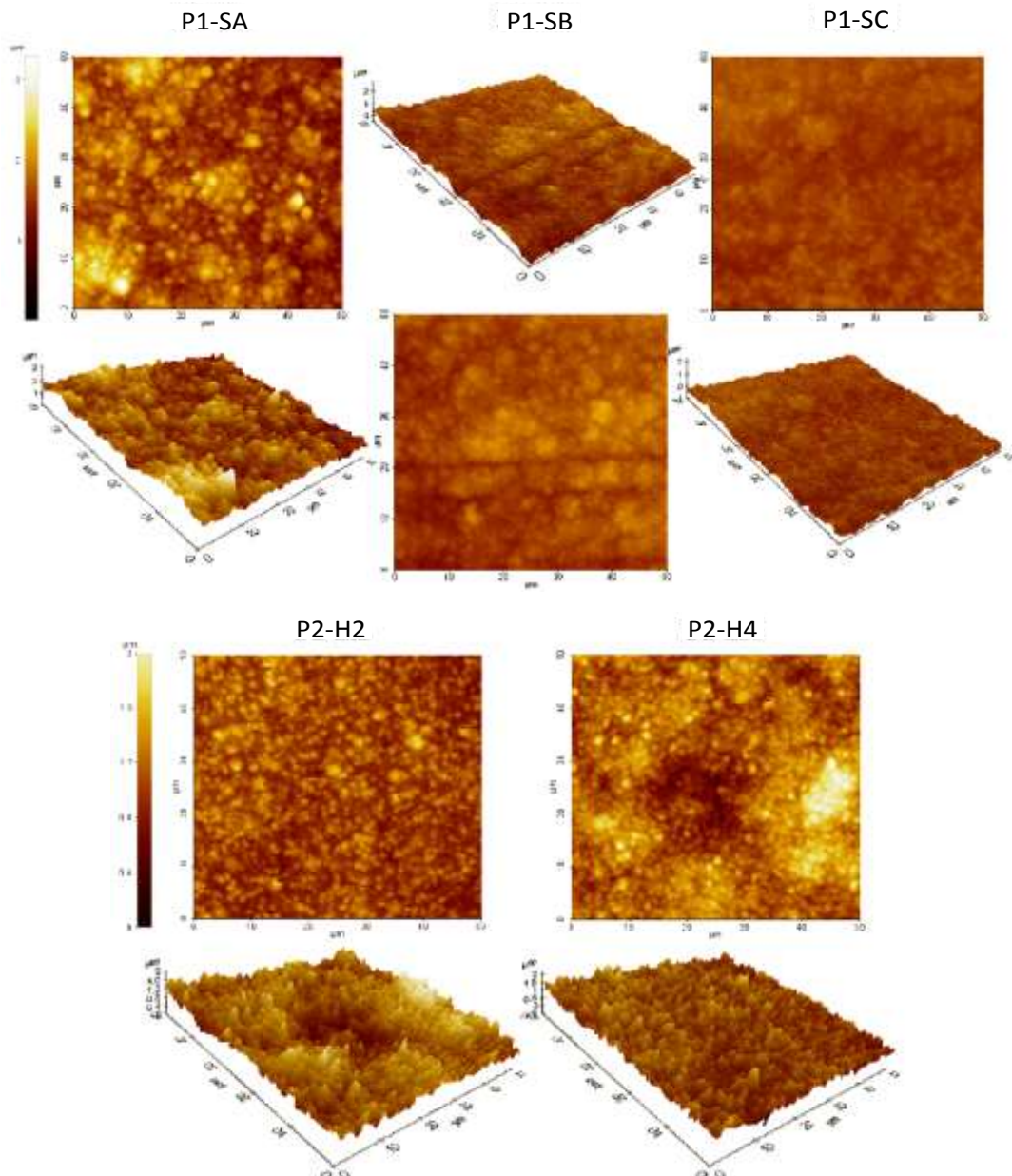
51

P1-SA   P1-SB   P1-SC

Fig. 5. Representative 2D and 3D AFM surface topography images of P1 (SA, SB, SC) and P2 (H2, H4).
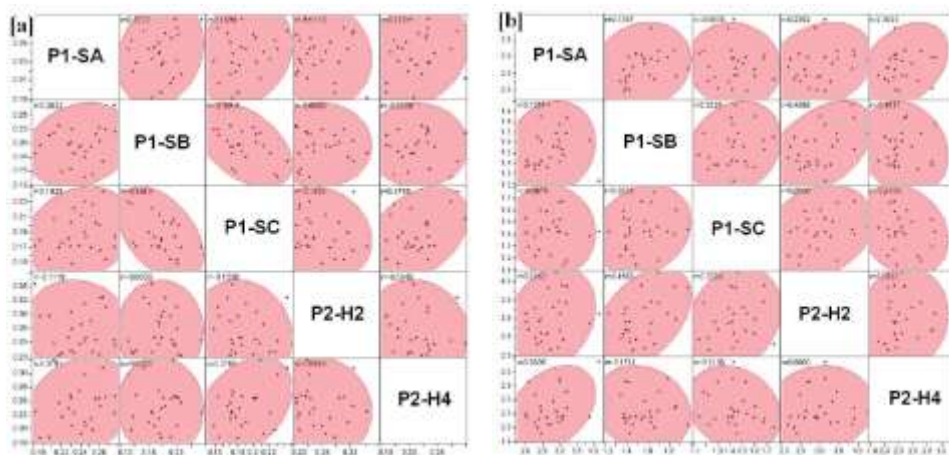

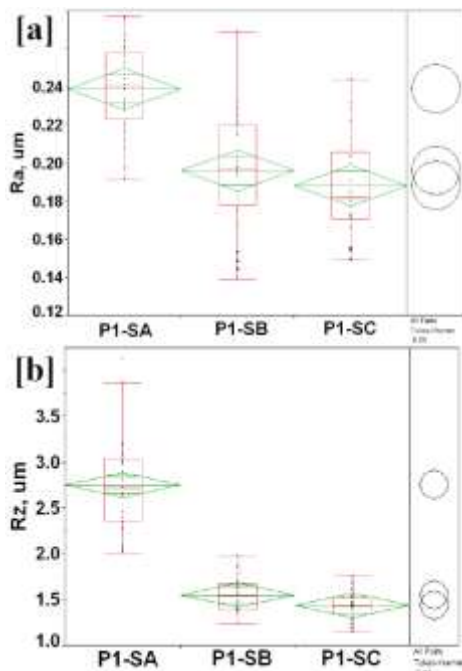
Fig. 6. Multivariate correlation for a) R_a, and b) R_z.

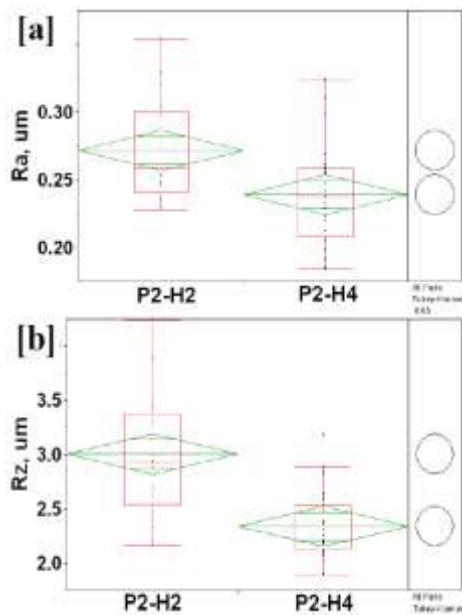Fig. 7. Comparative a) R_a and b) R_z values for P1.

Fig. 8. Comparative a) R_a and b) R_z values for P2.

Based from the results of the statistical analysis of the SR data where significant difference was found in some cases, correlation with NSOL occurrence can be established. Fig. 9 comparatively shows the level of NSOL in each case. It is clearly shown that high rate of NSOL is incurred when substrates with high SR is used regardless of the roughness parameter used. This observation unequivocally proves the strong empirical correlation of the two variables considered herein.
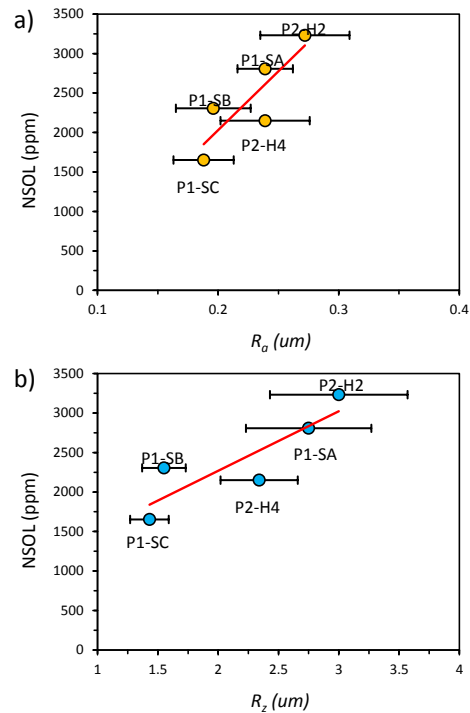

Fig. 9. Correlation of SR, a) R_a and b) R_z, with NSOL occurrence.

IV. CONCLUSION

NSOL is the top defect contributor on the wirebond yield reduction causing the yield to fall short of the 99.6% target; SR was identified as a probable cause. SR was measured using AFM in contact mode. Direct correlation has been established where high occurrence of NSOL was observed on substrates with high SR. This general correlation was found to be true for the two (2) packages evaluated in this study. R_a values of 0.192 ± 0.028 μm and R_z of 1.49 ± 0.18 μm were found to produce lower NSOL rate compared with R_a value of 0.239 ± 0.023 μm and R_z of 2.75 ± 0.52 μm for P1. Likewise, R_a of 0.272 ± 0.037 μm and R_z of 3.00 ± 0.57 μm were found to have higher occurrence of NSOL compared with R_a of 0.239 ± 0.037 μm and R_z of 2.34 ± 0.32 μm for P2. Based from the results presented herein, it is strongly recommended to expand the scope of the study, and to assess the universality of this correlation. Likewise, discussions with suppliers to reduce the SR of the substrates should be initiated. Specification needs to be established with respect to nominal values and the range, to use it as a control to reduce NSOL occurrence, eventually leading to the increase in the WB process yield.

REFERENCES

[1] Srikanth N, Murali S, Wong YM, Vath III CJ. Critical study of thermosonic copper ball bonding. Thin Solid Films, 2004, 462-463, 339-345.

[2] Oberhammer J, Stemme G. Active opening force and passive contact force electrostatic switches for soft metal contact materials. J. Microelectromech. Syst. 2005, 15, 1235-1242.

[3] Kassamakov I Vl, Seppänen HO, Oinonen, MJ, Hæggström, EO, Österberg JM, Aaltonen JP, Saarikko, H, Radivojevic ZP. Scanning white light interferometry in quality control of single-point tape automated bonding. Microelectron. Eng. 2007, 84, 114-123.

[4] Zhong Z, Goh KS. Analysis and experiments of ball deformation for ultra-fine-pitch wire bonding. J. Electron. Manuf., 2000, 10, 211-217.

[5] Jang C, Han S, Kim H, Kang S. A numerical failure analysis on lead breakage issues of ultrafine pitch flip chip-on-flex and tape carrier packages during chip/film assembly process. Microelectron. Reliab. 2006, 46, 487-495.

[6] Arulvanan P, Zhong Z, Shi X. Effects of process conditions on reliability, microstructure evolution and failure modes of SnAgCu solder joints. Microelectron. Reliab. 2006, 46, 432-439.

[7] Peters J, Vanherck P, Sastrodinoto M. Assessment of surface topology analysis techniques. CIRP Annals – Manufac. Technol., 1979, 28, 539-554.

[8] Sherrington I, Smith EH. The significance of surface topography in engineering. Precision Eng., 1986, 8, 79-87.

[9] Sherrington I, Smith EH. Modern measurement techniques in surface metrology: part I; stylus instruments, electron microscopy and non-optical comparators. Wear, 1988, 125, 271-288.

[10] Thwaite EG. Measurement and control of surface finish in manufacture. Precision Eng., 1984, 6, 207-217.

[11] Han X, Chen X, Yang X, Bai H, Li Z, Su X. Application of atomic force microscopy on the nanometer scale surface roughness measurement. Proc. 1st IEEE Intl Conf Nano/Micro Engineered and Molecular Systems, 1st IEEE-NEMS, 2006, art. no. 4134919, 131-135.

[12] Binnig G, Rohrer H, Gerber C, Weibel E. Vacuum tunneling. Physica B+C, 1982, 109-110, 2075-2077.

[13] Binnig G, Rohrer H, Gerber C, Weibel E. 7×7 Reconstruction on Si(111) Resolved in Real Space. Phys. Rev. Lett., 1983, 50, 120-123.

[14] Japanese Industrial Standards B 0601 (1994) and Japanese Industrial Standards B 0031 (1994).